NISTIR 6458

Characterization of the Inlet Combustion Air in NIST's Reference Spray Combustion Facility: Effect of Vane Angle and Reynolds Number

John F. Widmann
S. Rao Charagundla
Cary Presser

U.S. DEPARTMENT OF COMMERCE
Technology Administration
Process Measurements Division
Chemical Science and Technology Laboratory
National Institute of Standards and Technology
100 Bureau Drive
Gaithersburg, MD 20899

NIST

U.S. DEPARTMENT OF COMMERCE
Technology Administration
National Institute of Standards and Technology

NISTIR 6458

Characterization of the Inlet Combustion Air in NIST's Reference Spray Combustion Facility: Effect of Vane Angle and Reynolds Number

John F. Widmann
S. Rao Charagundla
Cary Presser

U.S. DEPARTMENT OF COMMERCE
Technology Administration
Process Measurements Division
Chemical Science and Technology Laboratory
National Institute of Standards and Technology
100 Bureau Drive
Gaithersburg, MD 20899

January 2000

U.S. DEPARTMENT OF COMMERCE
William M. Daley, Secretary

TECHNOLOGY ADMINISTRATION
Dr. Cheryl L. Shavers, Under Secretary of Commerce for Technology

NATIONAL INSTITUTE OF STANDARDS AND TECHNOLOGY
Raymond G. Kammer, Director

Contents

Notation

$C_{1\varepsilon}$, $C_{2\varepsilon}$, C_μ	constants in turbulence model equations
D_0	inner diameter of the outer pipe of the annular regions
D_i	outer diameter of the inner pipe of the annular regions
F_i	body forces
G_k	generation of k due to turbulent stresses
G_θ	axial flux of angular momentum
G_z	axial flux of axial momentum
k	turbulent kinetic energy
L	characteristic length
p	static pressure
r	radial coordinate
R_0	radial location of the outer wall of the annular passages
$\mathrm{Re} = (D_0 - D_i)\overline{u_z}/\nu$	Reynolds number
R_i	radial location of the inner wall of the annular passages
S	swirl number
t	time
u, $\overline{u}$	mean velocity
u_i, u_j, u_k	velocity components in Cartesian coordinates
u_θ	tangential velocity component
u_z	axial velocity component
$\overline{u_z}$	mean axial velocity based upon the volumetric flow rate
x_i, x_j, x_k	Cartesian coordinates
z	axial coordinate

Greek letters

α	vane angle defined in Fig. 3B
δ_{ij}	Kronecker delta
ε	turbulence dissipation rate
ν	kinematic viscosity
μ	viscosity
μ_t	eddy or turbulent viscosity
θ	polar angle
ρ	density
σ_k, σ_ε	constants in the turbulence model equations

Characterization of the Inlet Combustion Air in NIST's Reference Spray Combustion Facility: Effect of Vane Angle and Reynolds Number

John F. Widmann, S. Rao Charagundla, and Cary Presser
Chemical Science and Technology Laboratory
National Institute of Standards and Technology
100 Bureau Drive, Stop 8360
Gaithersburg, MD 20899-8360, USA

Abstract
The airflow through a 12-vane cascade swirl generator is examined numerically to characterize the inlet combustion air in the reference spray combustion facility at NIST. A three-dimensional model is used to simulate the aerodynamics in the swirl generator that imparts the desired degree of angular momentum to the air in the annulus leading into the reactor. A parametric study is presented in which the effects of the vane angle and Reynolds number are examined.† Reynolds numbers ranging from 5,000 to 30,000, and vane angles ranging from 30° to 60°, are investigated. For a vane angle of 50°, which is the current operating condition of the swirl generator, a recirculation zone develops at the exit of the annulus for Reynolds number, Re ≈ 9500. The Renormalization Group method (RNG) k-ε turbulence model is used to model the transport, production, and dissipation of turbulence due to its superior performance (relative to the standard k-ε turbulence model) for this type of flow.

Keywords: Swirl Number, Turbulence, Fluid Mechanics, Numerical Analysis, Code Validation, CFD, Reynolds Number

Introduction

The design and optimization of multiphase thermal oxidation systems in the power generation, waste incineration, and chemical process industries are relying increasingly on computational fluid dynamics (CFD) models and simulations to provide relevant process information in a cost-effective manner. In general, there is a need for experimental data with quantitative uncertainties that detail the characteristics of the droplet field and flame structure, and provide an understanding of their interrelationship with the system operating conditions. Of particular concern to modelers, and the motivation of this work, is the quantification of the boundary conditions, and especially the inlet conditions, to which numerical simulations are so sensitive. To meet this demand, the National Institute of Standards and Technology (NIST) has developed a reference spray combustion facility. A benchmark experimental database is being amassed that can be used for input and validation of multiphase combustion models and submodels (Widmann *et al.*, 1999a). As part of this program, our current focus is to provide parametric information on the aerodynamics at the inlet boundary (i.e., spatial

† Electronic files of the data presented in this report are available. Contact Cary Presser at *cpresser@nist.gov*.

profiles of the mean velocity components and turbulence intensity) that can be of value to the CFD modeler. In this report, a computational study was performed to investigate the effect of vane angle and Reynolds number on the inlet combustion air of NIST's reference spray combustion facility. The aerodynamics of the entering combustion air have a significant effect on the structure and stability of the spray flame. It is therefore crucial that this aspect of the reactor be adequately characterized if the facility is to be used for CFD validation. There was a two-fold justification for taking a computational approach. Firstly, to provide the flow through the burner and aerodynamic characteristics at the burner exit (or inlet condition of the chamber). This allowed comparison with experimental measurements of the mean velocity components, and provided turbulent intensity levels at the inlet boundary (before completion of the experimental measurements) for the modelers. Secondly, to clarify discrepancies between values of the swirl number derived from empirical geometric relationships and values computed from the surface integral equation that defines the swirl number.

In addition, a parallel program at NIST is underway to develop a reference atomizer that produces a spray with well-controlled characteristics. Such an atomizer would provide well-characterized inlet conditions for model validation, and would also permit testing, validation, and development of a variety of diagnostic techniques. Several industrial collaborators (e.g., Fluid Jet Associates, Creare Inc., CFD Research Corp.) are developing atomizers for this purpose, using acoustic and electrostatic atomization techniques. Of concern with the use of such an atomizer will be the interaction between the fuel transport processes and combustion air aerodynamics. Thus, a detailed description of the inlet combustion air flow field, corresponding to both present and future operating conditions, is required in anticipation of the needs of both the modeler and nozzle designer. This report has been prepared to address this issue.

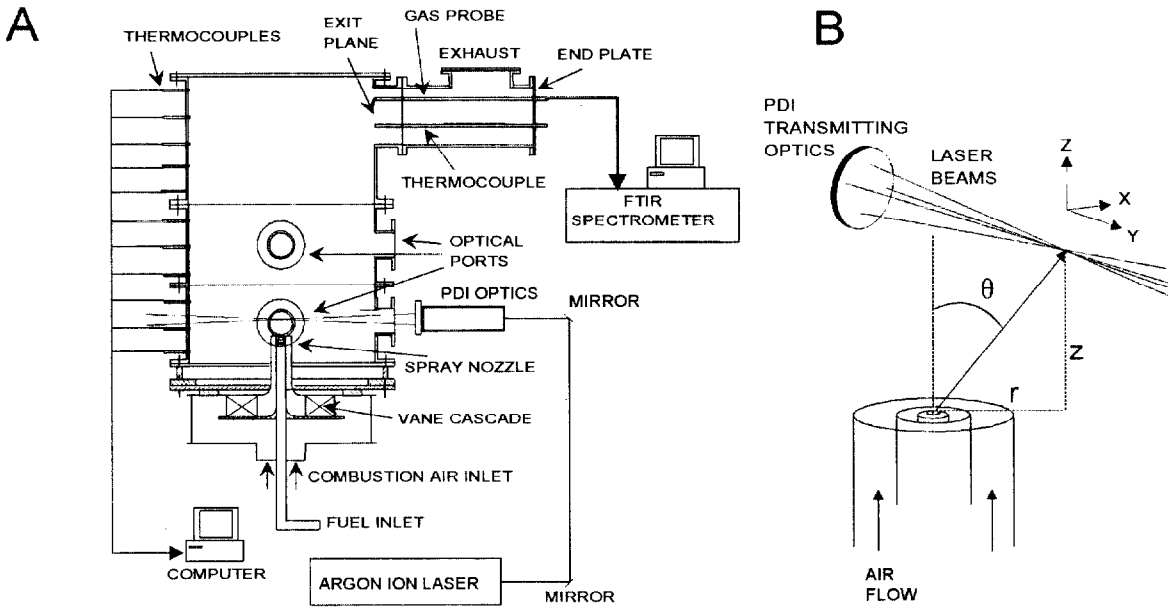

Fig. 1 Schematic of the (A) reference spray combustion facility at NIST, and (B) annulus surrounding the fuel nozzle through which the combustion air enters the reactor.

Reference Spray Combustion Facility

The experimental facility, shown in Fig. 1A, includes a swirl burner with a movable 12-vane swirl cascade. The cascade is adjusted to impart the desired degree of swirl intensity to the combustion air stream that passes through a 0.10 m o.d. passage and flows along the fuel passage. The swirl intensity is a measure of the angular momentum of the combustion air. It is characterized by the swirl number, S, defined as the ratio of the axial flux of angular momentum to the axial flux of axial momentum (Gupta et al., 1984). The swirl number in the annular region of the generator depends upon the vane angle and the Reynolds number, $Re = (D_0 - D_i)\overline{u_z}/\nu$.

Figure 1B presents an expanded view of the burner and nozzle. The nozzle is interchangeable, and a variety of fuels can be used in the facility. The fuel flow rate, combustion air flow rate, wall temperatures, and exiting gas temperatures are monitored and stored on a personal computer.

The burner is enclosed within a stainless steel chamber to provide improved reproducibility and control of the spray flame. The chamber height is 1.2 m and the inner diameter is 0.8 m. Several windows provide optical access for nonintrusive probing of the flame. A stepper-motor-driven traversing system translates the entire burner/chamber assembly and thus permits measurements of spray properties at selected locations downstream of the nozzle. Additional details on the design of the burner are available in the literature (Presser et al., 1993). The relevant dimensions necessary for modeling the facility are presented in Fig. 2. Note that the reactor exit is off-axis, which makes the problem non-axisymmetric.

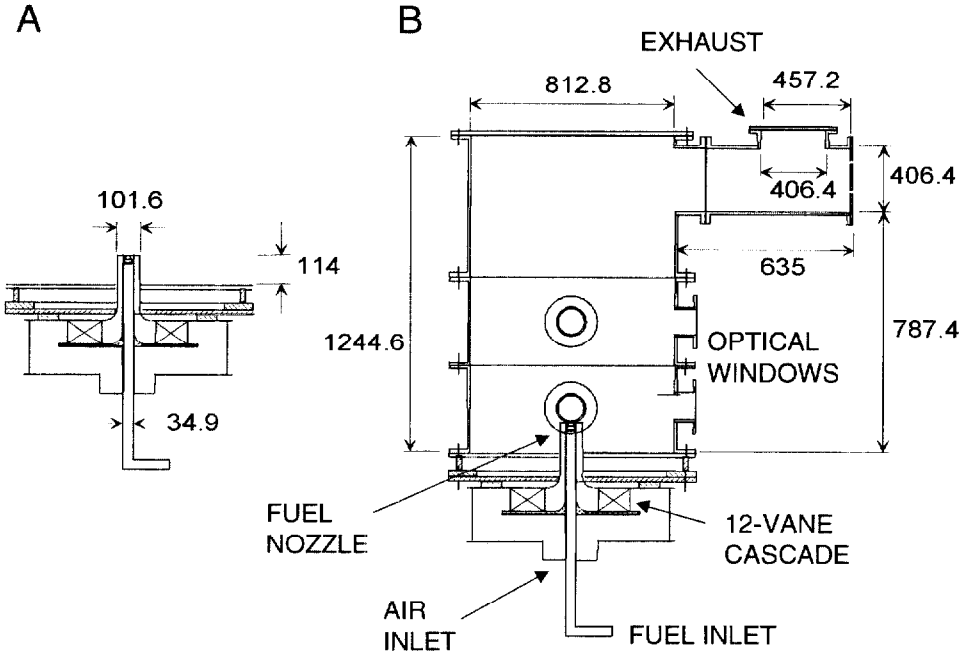

Fig. 2 Schematic of (A) the 12-vane cascade swirl generator, and (B) the spray combustion facility. Dimensions are given in millimeters.

In this paper, the airflow through the vane-cascade swirl generator, shown in Fig. 2A, was simulated using FLUENT† computational fluid dynamics software (FLUENT Inc., 1998). Recently, Widmann *et al.* (1999b) modeled the airflow through the swirl generator using two turbulence models, the standard k-ε model (Launder and Spalding, 1972) and the Renormalized Group theory (RNG) k-ε model (Yakhot and Orszag, 1986), at conditions corresponding to the baseline case of the NIST database (50° vane angle and Re = 10,000). The two turbulence models are two equation models in which two scalar transport equations are used to describe the production, diffusion, and dissipation of turbulence.

The standard k-ε model is a semi-empirical turbulence model based upon an isotropic eddy-viscosity hypothesis. It is widely used in industrial flow and heat transfer simulations due to its robustness, economy, and reasonable accuracy (Shyy *et al.*, 1997). The RNG k-ε model also belongs to the k-ε family of turbulence models; however, unlike the standard k-ε model, the RNG k-ε model was derived using a statistical technique called renormalization group methods. The model equations are similar to the standard k-ε model, but the statistical derivation results in different values for the various constants in the equations.

Smith and Reynolds (1992) reported inaccuracies with the specific values of the constants in the RNG k-ε model. In response, Yakhot and coworkers reformulated the earlier derivation of the differential equation describing the transport of ε (Yakhot *et al.*, 1992; Yakhot and Smith, 1992). With this change, the RNG k-ε turbulence model has shown improvement over the standard k-ε model when applied to many industrial flows (e.g., Papageorgakis and Assanis, 1999; Yin *et al.*, 1996; Lien and Leschziner, 1994; Yakhot *et al.*, 1992). Particularly, noteworthy is the rate-of-strain term in the transport equation for ε that has been reported to result in improved predictions of flow fields with high strain rates. In particular, flows in curved geometries, stagnation flows, separated flows, and swirling flows are situations in which the RNG k-ε model has been reported to be more accurate than the standard k-ε turbulence model. Benim (1990) compared the performance of these two turbulence models in a swirling combustor and found that the RNG k-ε model resulted in predictions consistent with experiment, while the standard k-ε model compared poorly with the experimental data. Widmann *et al.* (1999b) applied both of these turbulence models to simulations of airflow through the vane-cascade swirl generator shown in Fig. 2A, including the swirling flow through the annulus following the vanes. They found that only the RNG k-ε model resulted in predicted flowfields consistent with experimental data.

Numerical Methodology

The numerical formulation is for isothermal, turbulent airflow through the 12-vane cascade swirl generator shown in Fig. 2A. The relevant conservation equations include continuity, the Reynolds averaged Navier-Stokes equations, and an appropriate turbulence model. The Reynolds averaged Navier-Stokes equations are generated from

† Certain commercial equipment, materials, or software are identified in this publication to specify adequately the experimental procedure. Such identification does not imply recommendation or endorsement by the National Institute of Standards and Technology, nor does it imply that the materials or equipment are necessarily the best available for this purpose.

the instantaneous Navier-Stokes equations using the following transformations (Bird *et al.*, 1960):

$$u_i = \overline{u}_i + u'_i, \quad \rho = \overline{\rho} + \rho', \text{ and } \quad p = \overline{p} + p'. \tag{1}$$

Here, the overbar and prime indicate a time-averaged quantity and an instantaneous fluctuation, respectively. Dropping the overbar for convenience, the resulting expression for the momentum equation in Cartesian coordinates is

$$\frac{\partial}{\partial t}(\rho u_i) + \frac{\partial}{\partial x_j}(\rho u_i u_j) = -\frac{\partial p}{\partial x_i} + \frac{\partial}{\partial x_j}\left[\mu\left(\frac{\partial u_i}{\partial x_j} + \frac{\partial u_j}{\partial x_i}\right) - \frac{2}{3}\mu\frac{\partial u_k}{\partial x_k}\delta_{ij}\right] + F_i + \frac{\partial}{\partial x_j}(-\rho\overline{u'_i u'_j}). \tag{2}$$

The last term in Eq. (2) is the derivative of the *Reynolds stresses*, $-\rho\overline{u'_i u'_j}$, and represents the effect of turbulence on the momentum balance. The Reynolds stresses represent additional unknowns, and a set of constitutive equations is required to close these equations. The turbulence models provide the additional equations necessary to close the transport equations.

The Reynolds stresses in Eq. (2) are computed using the Boussinesq hypothesis (Hinze, 1975),

$$-\rho\overline{u_i u_j} = \mu_t\left(\frac{\partial u_i}{\partial x_j} + \frac{\partial u_j}{\partial x_i}\right) - \frac{2}{3}\left(\rho k + \mu_t\frac{\partial u_i}{\partial x_i}\right)\delta_{ij}, \tag{3}$$

where μ_t is the *eddy* or *turbulent viscosity* computed from

$$\mu_t = \rho C_\mu \frac{k^2}{\varepsilon}. \tag{4}$$

For the standard k-ε turbulence model, the scalar quantities k and ε are computed from the following transport equations:

$$\frac{\partial}{\partial t}(\rho k) + \frac{\partial}{\partial x_i}(\rho u_i k) = \frac{\partial}{\partial x_i}\left[\left(\mu + \frac{\mu_t}{\sigma_k}\right)\frac{\partial k}{\partial x_i}\right] + G_k - \rho\varepsilon \tag{5}$$

and

$$\frac{\partial}{\partial t}(\rho\varepsilon) + \frac{\partial}{\partial x_i}(\rho u_i \varepsilon) = \frac{\partial}{\partial x_i}\left[\left(\mu + \frac{\mu_t}{\sigma_k}\right)\frac{\partial \varepsilon}{\partial x_i}\right] + C_{1\varepsilon}\frac{\varepsilon}{k}G_k - C_{2\varepsilon}\rho\frac{\varepsilon^2}{k}. \tag{6}$$

The generation of k due to turbulent stresses, G_k, is given by

$$G_k = -\rho\overline{u_i u_j}\frac{\partial u_j}{\partial x_i}. \tag{7}$$

The values of the constants in Eqs. (4) - (6) have been determined experimentally to be $C_{1\varepsilon} = 1.44$, $C_{2\varepsilon} = 1.92$, $C_\mu = 0.09$, $\sigma_k = 1.0$, and $\sigma_e = 1.3$ (Launder and Spalding, 1972).

The numerical simulations carried out in this study were generated using a segregated, implicit solver. Integrating the transient problem to steady state was found to be computationally less expensive than solving the time-independent transport equations, and this method was used for the results presented here. The coupled equations were solved with first order accuracy in time and second order accuracy in momentum, continuity, and turbulence parameters. The pressure and velocity were coupled using the PISO algorithm (Issa, 1986) with neighbor and skewness correction, and standard wall functions (Launder and Spalding, 1974) were used for the near-wall treatment.

A uniform velocity profile was used for the inlet condition, and an inlet turbulence intensity of 10 % was assumed with a characteristic length of $R_0 - R_i = 0.0333$ m. The predictions at the outlet of the domain were not sensitive to the inlet turbulence intensity. In this report, the Reynolds number, based upon the mean axial velocity in the annular regions of the domain, was varied from 5,000 to 30,000. Sheen *et al.* (1997) reported the transition from laminar to turbulent flow in an annulus to occur at $Re \approx 1600$; therefore, we expect fully developed turbulent flow for all of these simulations. At the outlet, the radial velocity was assumed negligible and the radial equilibrium pressure distribution was calculated by

$$\frac{\partial p}{\partial r} = \frac{\rho u_\theta^2}{r}. \tag{8}$$

Also at the outlet, the turbulence intensity and characteristic length used for the inlet condition were assumed in the event of backflow into the domain, such as in a recirculation zone.

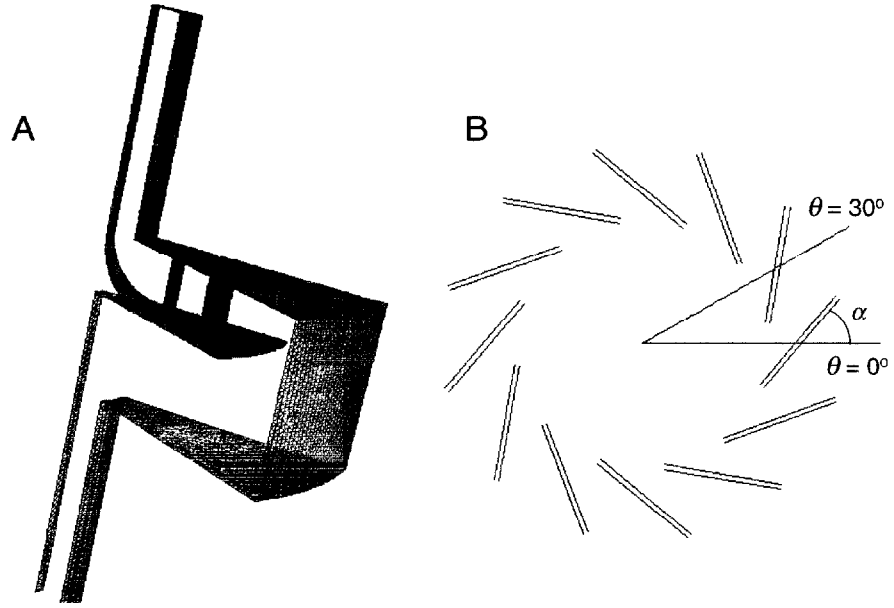

Fig. 3 Schematic of (A) the surface mesh used to generate the unstructured grid for the numerical simulation, and (B) a top view of the 12-vane cascade and the modeled 30° section. Note that the periodic boundaries in (A) have been omitted for clarity.

A three-dimensional model is required for this geometry; however, due to symmetry it is only necessary to simulate a 30° portion of the vane cascade. An unstructured grid was used for the simulations, and the surface mesh is shown in Fig. 3A. Note that the rotationally periodic symmetry planes at $\theta = 0^{\circ}$ and $\theta = 30^{\circ}$ are not shown in the figure. The mesh was constructed so that the grid resolution gradually increased from the inlet to the vanes, and then remained high throughout the remainder of the domain. The number of cells in the mesh was systematically increased until the solution was determined to be grid-independent, and this strategy of gradually increasing the resolution from the inlet plane to the vanes was used for all of the grids. The predictions presented here correspond to results obtained from a grid with approximately 277,000 cells. A top view of the vanes is shown in Fig. 3B, and the 30° section that was modeled is depicted. The vane angle, α, is shown in the figure.

Results

The combustion air is assumed to enter at the bottom of the swirl generator with a uniform velocity profile. The air flows through an annular section approximately 0.178 m long with the same radial dimensions as the exit annulus (R_i = 0.0175 m and R_0 = 0.0508 m). The flow is then directed radially outward (see Fig. 1A). The flow bends upward and then returns toward the center of the swirl generator as it passes through the vanes. The swirling flow is finally directed upward through the exit annulus, approximately 0.165 m long, and enters the reactor. The fuel is introduced into the reactor through the inner passage of the annulus (see Fig. 1B); therefore, the swirling combustion air flows around the fuel nozzle as it enters the reactor.

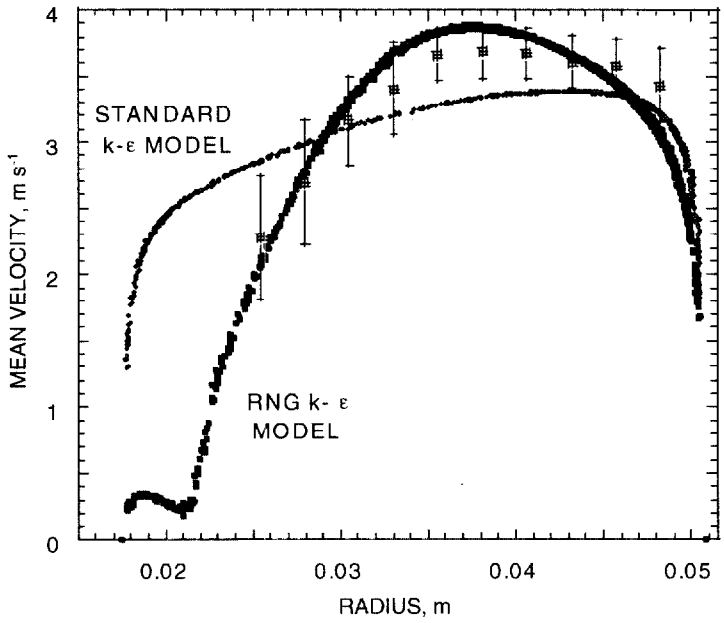

Fig. 4 Variation for the total air velocity with radial position at the annulus outlet. The experimental data are compared to the numerical simulation using the standard and RNG k-ε turbulence models.

Figure 4 presents the variation of total air velocity with radial position at the annulus outlet. The predicted velocity profiles are compared with the experimental data of Widmann *et al.* (1999b) for a vane angle, α, of 50° and Re = 10,000. The error bars in the figure correspond to combined standard uncertainties with a coverage factor of 2 (Taylor and Kuyatt, 1994). Additional details of the uncertainty analysis can be found elsewhere (Widmann *et al.*, 1999b). As shown in Fig. 4, the standard k-ε model is in poor agreement with the experimental data, failing to predict the recirculation zone present at the outlet. The RNG k-ε turbulence model predicts the recirculation zone that is experimentally observed, and the predicted velocity profile agrees well with the experimental data. For this reason, all of the simulations presented in this report used the RNG k-ε turbulence model.

CASE	VANE ANGLE	REYNOLDS NUMBER	SWIRL NUMBER
1	30°	10,000	0.28
2	30°	20,000	0.28
3	40°	5,000	0.35
4	40°	10,000	0.35
5	40°	20,000	0.35
6	50°	5,000	0.42
7	50°	7,500	0.43
8	50°	8,000	0.43
9	50°	8,500	0.43
10	50°	9,000	0.44
11	50°	9,500	0.49
12	50°	10,000	0.49
13	50°	15,000	0.50
14	50°	20,000	0.50
15	50°	30,000	0.51
16	60°	5,000	0.59
17	60°	10,000	0.63
18	60°	20,000	0.65
19	60°	30,000	0.66

Table 1 The set of vane angles and Reynolds numbers explored in this report. Data files are available that detail the profiles of total velocity, axial velocity, tangential velocity, static pressure, turbulence intensity, and turbulence parameters (k and ε) for each case.

The velocity profiles of the inlet combustion air were determined by simulating the airflow through the swirl generator for a variety of vane angles and Reynolds numbers. Vane angles of 30°, 40°, 50°, and 60° were studied, and the Reynolds number was varied from 5,000 to 30,000. A vane angle of 50° is currently being used in the facility, so this

angle was investigated to a greater extent than the other vane angles. Table 1 summarizes the different conditions for the 19 simulations. Data files for each case are available from the authors that detail the profiles of total velocity, axial velocity, tangential velocity, static pressure, turbulence intensity, and turbulence parameters (k and ε) at the outlet of the annulus (i.e., inlet of the spray combustion reactor).

The effect of the vane angle on the predicted radial profiles of total velocity, axial velocity, tangential velocity, and turbulence intensity for Re = 10,000 at the outlet plane of the simulation are shown in Figs. 5 - 8, respectively. Radial velocities are negligible for all cases. The total velocity profiles in Fig. 5 reveal that the highest velocities are near the inner wall of the annulus for vane angles of 30° and 40°. However, as the vane angle is increased, the radial coordinate corresponding to the maximum velocity moves towards the outer wall. In addition, a recirculation zone develops near the inner wall, and the size of the recirculation zone increases with increasing vane angle. Figure 6 indicates that the corresponding profiles of the axial velocity component follow essentially the same trends except that the radial coordinate corresponding to the maximum velocity is greater for $\alpha = 30°$ than for $\alpha = 40°$. The recirculation zone predicted by the simulations with vane angles of 50° and 60° is shown clearly in Fig. 6. For the simulations with a recirculation zone, the air flow is predominantly near the outer wall.

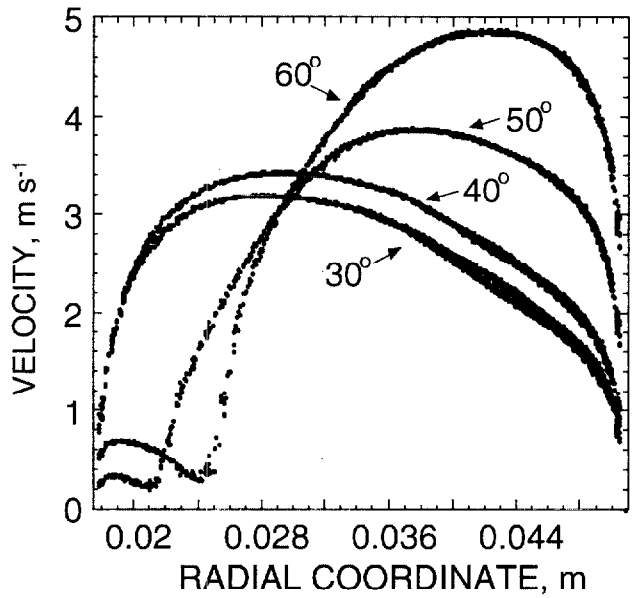

Fig. 5 Variation of the predicted total velocity with radial position at the outlet of the annulus for Re = 10,000 and vane angles, α, of 30°, 40°, 50°, and 60°.

The variation of the predicted tangential velocity component with radial position is presented in Fig. 7. The tangential velocity profiles, like the axial velocity profiles, peak near the inner wall for vane angles of 30° and 40°, but are shifted toward larger radial coordinates for vane angles of 50° and 60° due to the recirculation zone. At radial positions within the recirculation zone, the tangential velocity is negligible, indicating that the flow is essentially axial upstream into the burner passage. The variation of the

relative turbulence intensities with radial position are presented in Fig. 8. The simulations with vane angles of 30° and 40° predict turbulence intensities in the range of 20 % to 40 %. In contrast, the simulation with a 50° vane angle predicts turbulence intensities ranging from below 5 % to 50 %, and the simulation with α = 60° predicts turbulence intensities in the range 7 % to 70 %. The recirculation zone results in a region of high velocity gradients, and therefore high shear, that increases the turbulence levels appreciably.

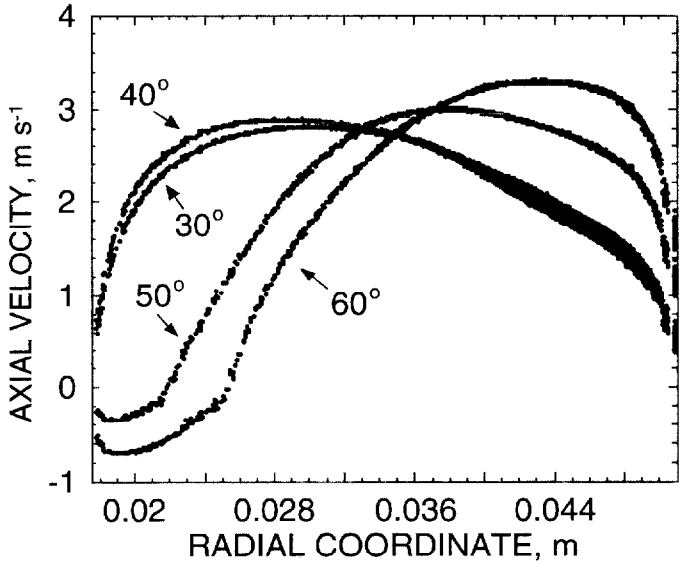

Fig. 6 Variation of the predicted axial velocity with radial position at the outlet of the annulus for *Re* = 10,000 and vane angles, α, of 30°, 40°, 50°, and 60°.

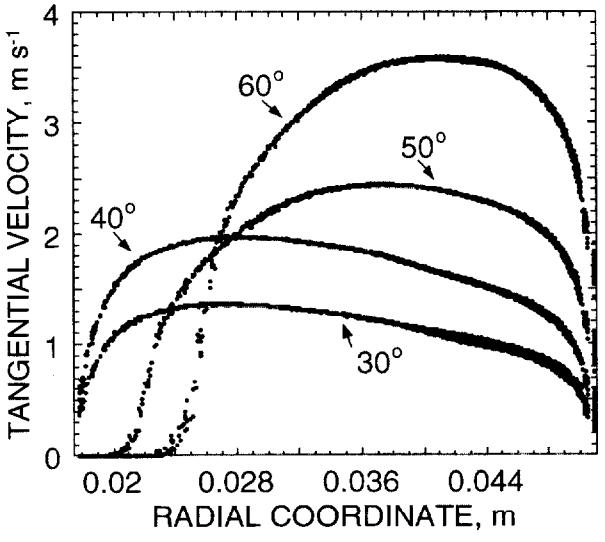

Fig. 7 Variation of the predicted tangential velocity with radial position at the outlet of the annulus for *Re* = 10,000 and vane angles, α, of 30°, 40°, 50°, and 60°.

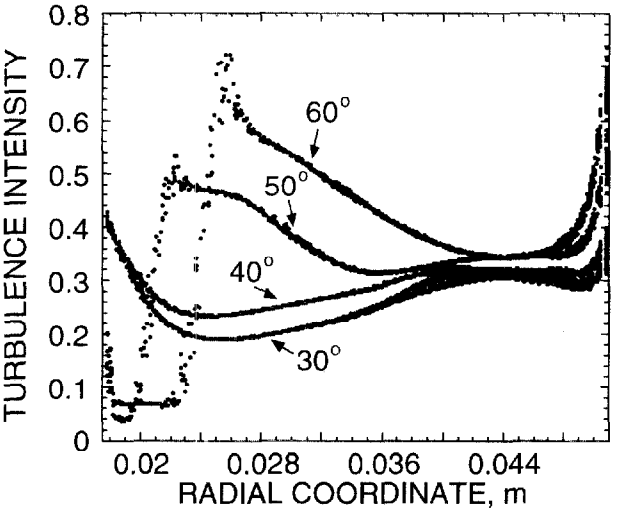

Fig. 8 Variaiton of the predicted turbulence intensity with radial position at the outlet of the annulus for Re = 10,000 and vane angles, α, of 30°, 40°, 50°, and 60°.

The variation of the inlet combustion air characteristics with Reynolds number is presented in Figs. 9 - 13. Profiles of total velocity, axial velocity, tangential velocity, turbulence intensity, and static pressure are presented, respectively, for six values of the Reynolds number and a vane angle of 50°. In each case, the profiles for Re = 5,000 and Re = 7,500 (Frames A and B) are similar, but considerably different from the remaining four profiles that correspond to the simulations predicting a recirculation zone (Frames C, D, E, and F). When comparing Fig. 5 with Fig. 9, it is clear that the effect of vane angle on the shape of the predicted radial profiles is more significant than the effect of Reynolds number. However, the magnitude of the velocity components, turbulence intensity, and static pressure depend strongly on Re.

Inlet Swirl number

The degree of swirl present in the combustion air entering a burner or furnace has a strong effect on the structure and stability of the flame, and it is therefore an important inlet parameter for modelers. Despite the importance of characterizing the swirling flow, several obstacles prevent the reliable prediction of highly swirling flow fields. As discussed above, one difficulty encountered when designing these systems is the questionable accuracy of current turbulence models for highly strained flows. This uncertainty results in flow field predictions that are suspect until validated with experimental data. In addition, geometrical and empirical correlations available in the literature are highly geometry dependent and often involve simplifying assumptions (e.g., inviscid flow) that lead to large uncertainties in the predictions.

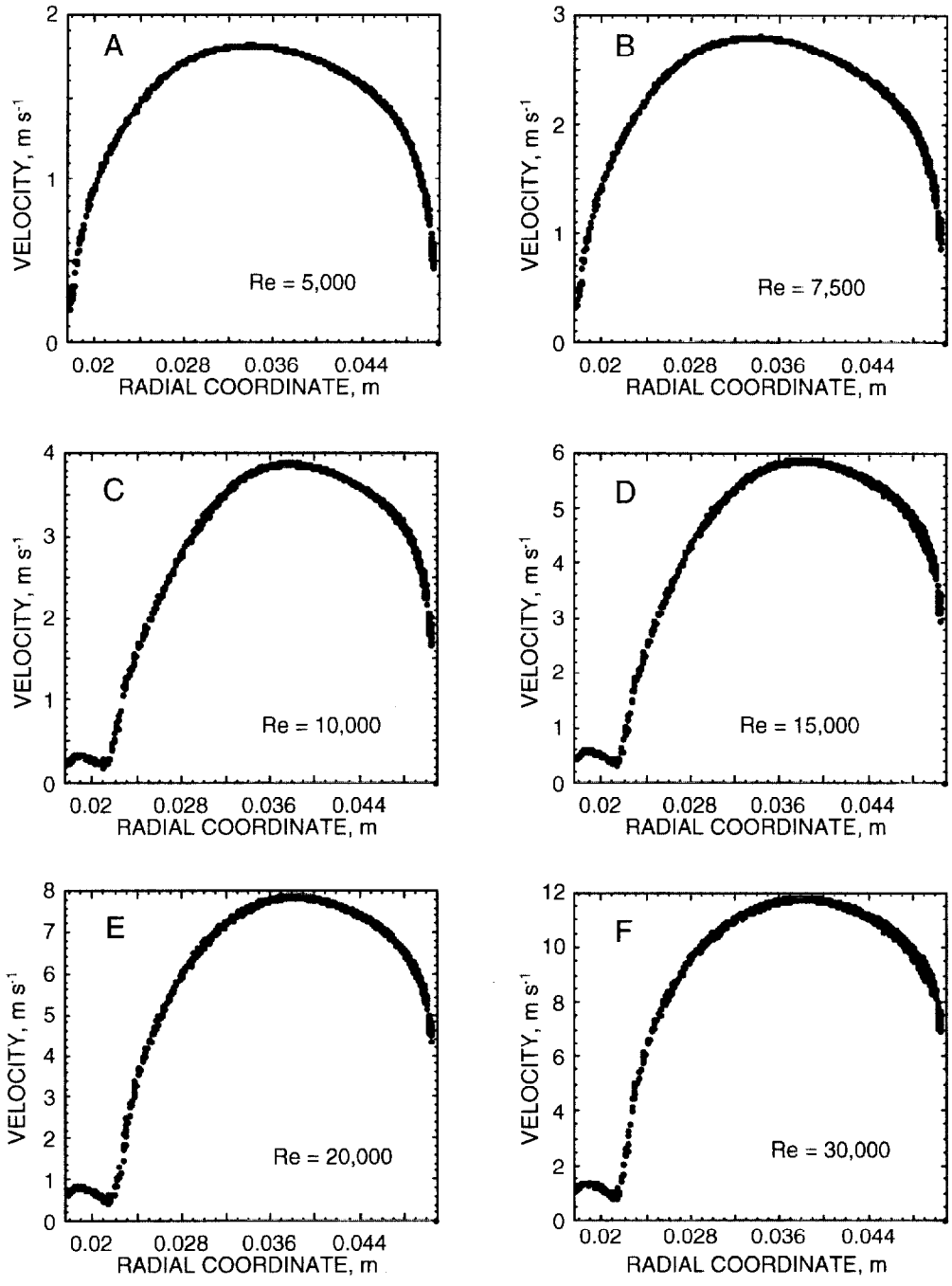

Fig. 9 Variation of the predicted total velocity with radial position at the outlet of the annulus for a vane angle, α, of 50° and various Reynolds numbers.

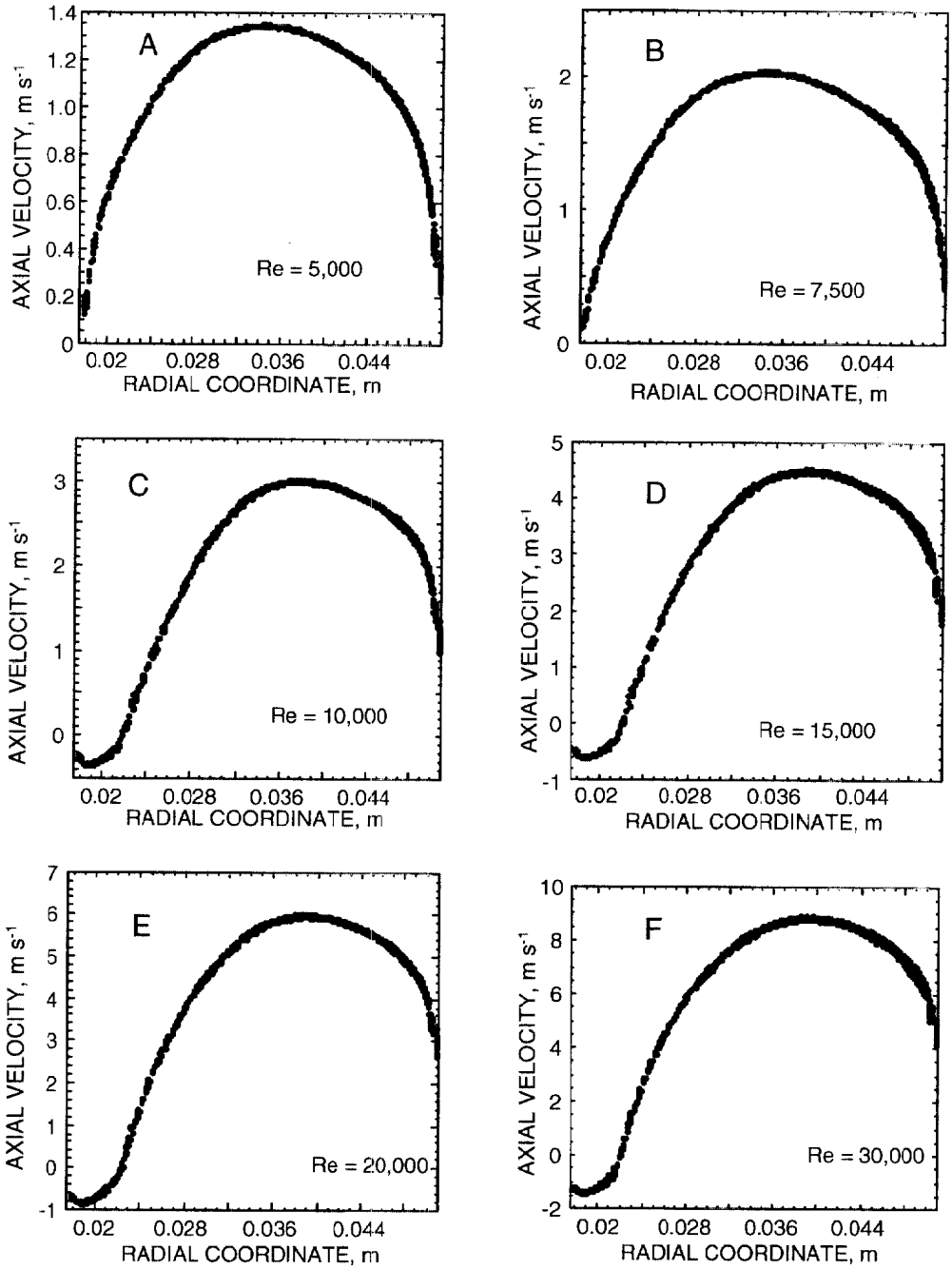

Fig. 10 Variation of the predicted axial velocity with radial position at the outlet of the annulus for a vane angle, α, of 50° and various Reynolds numbers.

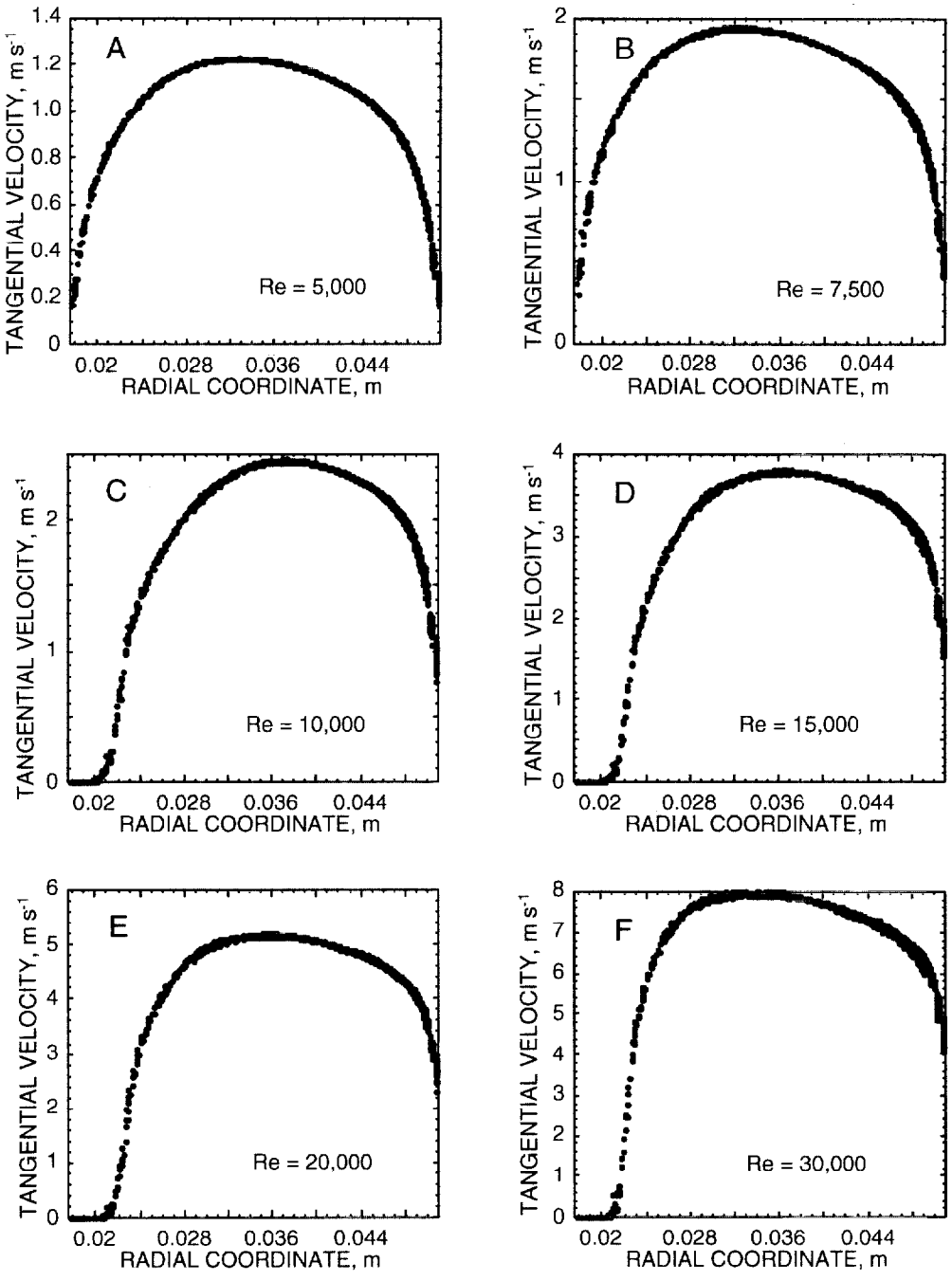

Fig. 11 Variation of the predicted tangential velocity with radial position at the outlet of the annulus for a vane angle, α, of 50^{o} and various Reynolds numbers.

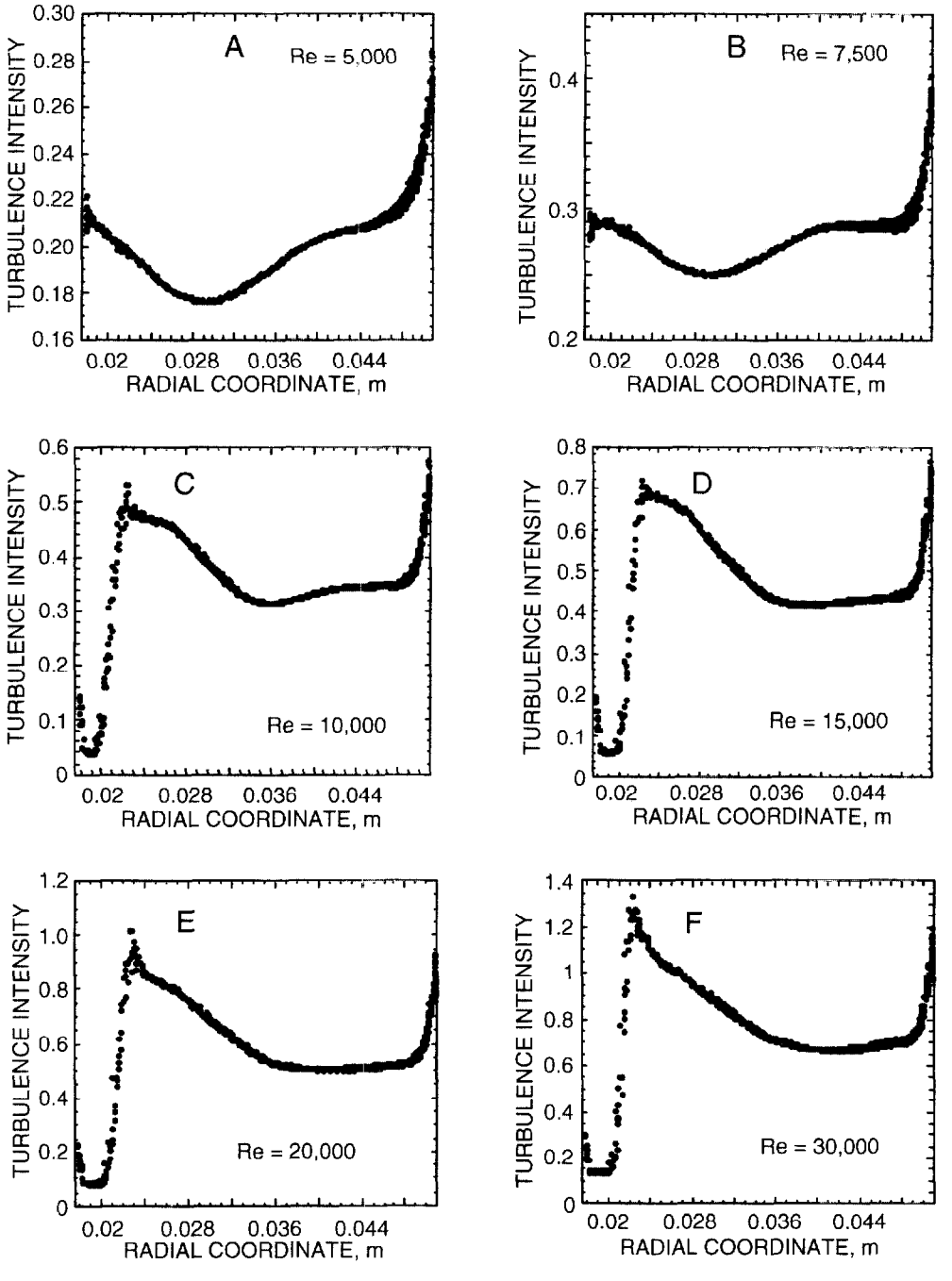

Fig. 12 Variation of the predicted turbulence intensity with radial position at the outlet of the annulus for a vane angle, α, of 50° and various Reynolds numbers.

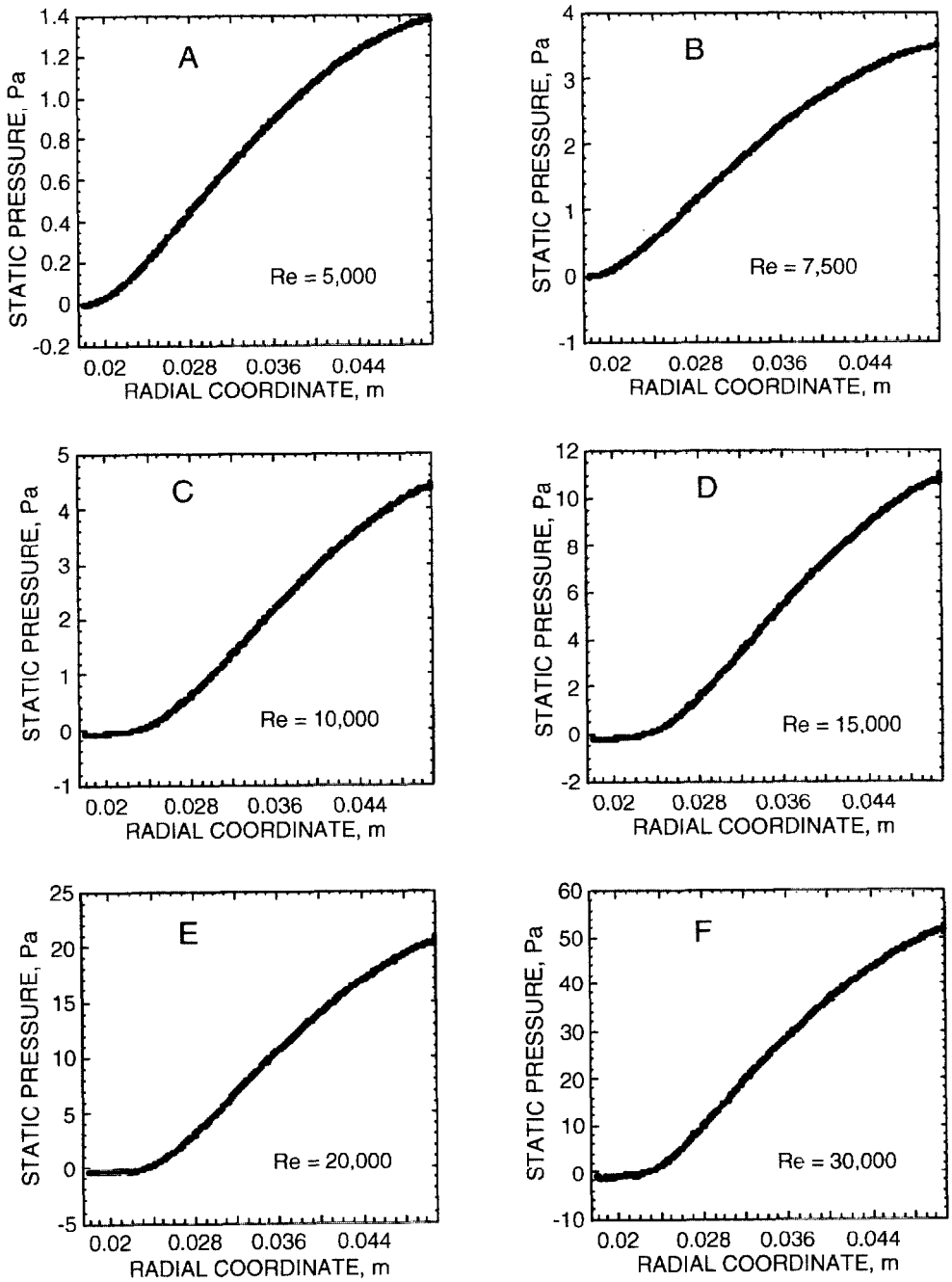

Fig. 13 Variation of the predicted static (gauge) pressure with radial position at the outlet of the annulus for a vane angle, α, of 50° and various Reynolds numbers.

The swirl number is a non-dimensional parameter that characterizes the degree of swirl present in the flow. It is defined as (Gupta *et al.*, 1984)

$$S = \frac{G_\theta}{LG_z} \tag{9}$$

where L is a characteristic length, typically chosen to be the exit radius of the burner. The terms G_θ and G_z are the axial flux of angular momentum and the axial flux of axial momentum, respectively, and are given by

$$G_\theta = \int_0^\infty \rho u_z u_\theta r^2 dr \tag{10}$$

and

$$G_z = \int_0^\infty (\rho u_z^2 + p) r dr \,. \tag{11}$$

Here u_z and u_θ are the axial and tangential velocity components, respectively. For the 12-vane swirl generator investigated in the present study, the characteristic length used was the radial coordinate of the outer wall of the annulus (see Fig. 1B), $L = R_0 = 0.0508$ m.

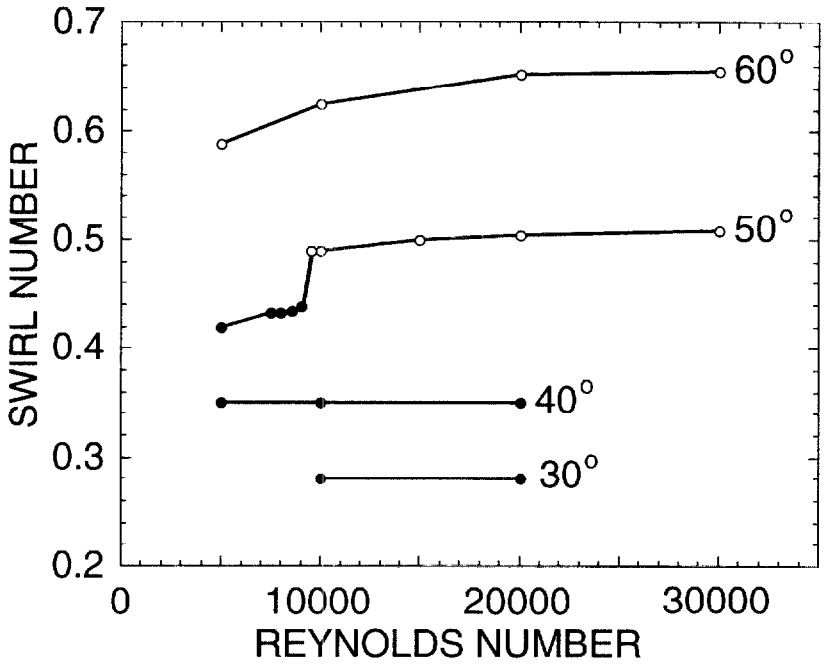

Fig. 14 Variation of the swirl number, S, calculated from Eqs. (9) - (11), with Reynolds number for each of the cases investigated. The vane angle, α, is indicated in the figure. The open symbols correspond to simulations in which a recirculation zone is predicted at the outlet.

Figure 14 presents the swirl number calculated at the outlet of the computational domain for each of the simulations in Table 1. The open symbols correspond to cases in which a recirculation zone was predicted at the outlet of the domain. For vane angles of 30° and 40°, the swirl number is independent of *Re* over the range of Reynolds numbers investigated, indicating that viscosity effects are not significant. For these vane angles, simulations and correlations invoking the inviscid assumption will likely give reasonable predictions. Note that the simulations corresponding to $\alpha = 30°$ or $\alpha = 40°$ do not predict the presence of a recirculation zone at the outlet of the domain. For the simulations with vane angles of 50° and 60°, the swirl number is a weak function of Reynolds number, but reaches asymptotic values for high Reynolds numbers.

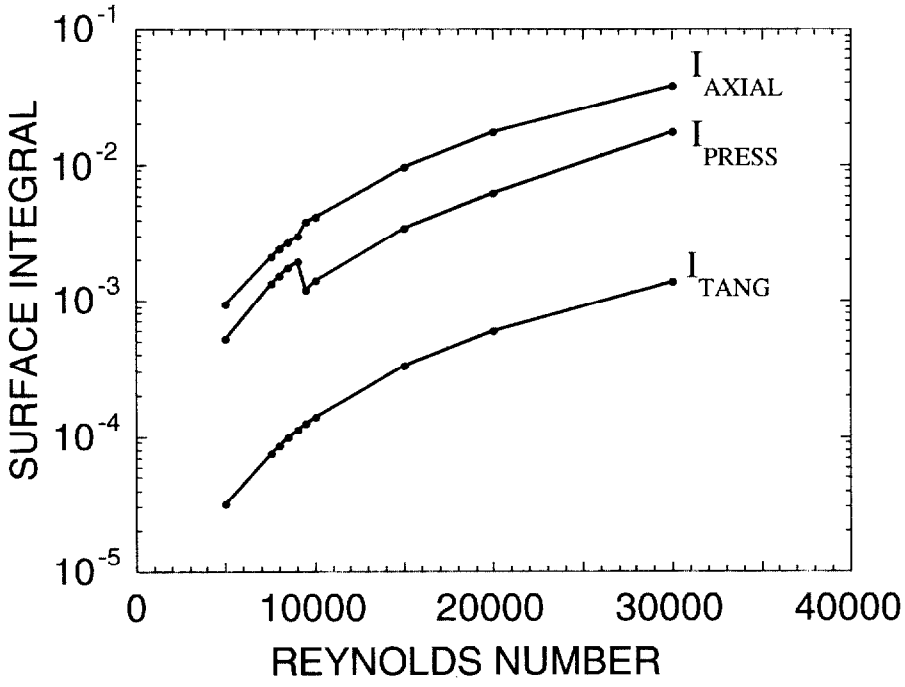

Fig. 15 Variation of the axial momentum (I_{AXIAL}), tangential momentum (I_{TANG}), and static pressure (I_{PRESS}) contributions to the swirl number calculation with Reynolds number.

The abrupt increase in the swirl number at Re ≈ 9,500 predicted for α = 50° corresponds to the development of a recirculation zone at the outlet, and results from a decrease in the static pressure contribution in Eq. (11), as shown in Fig. 15. The curves labeled I_{AXIAL}, I_{TANG}, and I_{PRESS} in Fig. 15 correspond to

$$I_{AXIAL} = \int_0^\infty \rho u_z^2 r dr, \tag{12}$$

$$I_{TANG} = G_\theta = \int_0^\infty \rho u_z u_\theta r^2 dr, \tag{13}$$

and

$$I_{PRESS} = \int_0^\infty pr dr, \tag{14}$$

respectively. The static pressure contribution to the swirl number, I_{PRESS}, decreases abruptly when the recirculation zone develops due to the negative static pressure in the recirculation zone. The decrease in I_{PRESS}, which appears in the denominator of Eq. (9), results in an abrupt increase in the swirl number.

Summary

The combustion air entering the reference spray combustion facility at NIST has been investigated computationally using the Reynolds averaged Navier-Stokes equations and the RNG k-ε turbulence model. The RNG k-ε turbulence model was previously validated experimentally for the confined, swirling flow studied in this investigation. A parametric study is presented in which the effects of the Reynolds number and vane angle are examined for the ranges of $5{,}000 < Re < 30{,}000$ and $30^\circ < \alpha < 60^\circ$. The simulations with a vane angle of 50°, which is the current operating condition for the reference spray combustion facility, predict the development of a recirculation zone for $Re \approx 9500$. This report completes a recent study intended to characterize the inlet combustion air in the NIST reference spray combustion facility. The details presented herein can be used as inlet conditions for modelers attempting to simulate the multiphase combustion process within the reactor.

Acknowledgements

The authors would like to thank Mike Carrier for technical support. One of the authors (JFW) wishes to acknowledge the financial support of the NRC/NIST Postdoctoral Research Program.

References

Benim, A. C. (1990). Finite Element Analysis of Confined Turbulent Swirling Flows. *International Journal of Numerical Methods in Fluids.* **11**:697-717.

Bird, R. B., Stewart, W. E., and Lightfoot, E. N. (1960). *Transport Phenomena*, John Wiley & Sons, New York.

Fluent 5 User's Guide. (1998). Fluent Incorporated, Lebanon, NH 03766 USA.

Gupta, A. K., Lilley, D. G., and Syred, N. (1984). *Swirl Flows*, Abacus Press, Kent.

Hinze, J. O. (1975). *Turbulence*, McGraw-Hill Publishing Co., New York.

Issa, R. I. (1986). Solution of Implicitly Discretized Fluid Flow Equations by Operator Splitting. *Journal of Computational Physics.* **62**:40-65.

Jaw, S. Y., and Chen, C. J. (1998). Present Status of Second-Order Closure Turbulence Models. I: Overview. *Journal of Engineering Mechanics.* **124**:485-501.

Launder, B. E., and Spalding, D. B. (1972). *Lectures in Mathematical Models of Turbulence*, Academic Press, London.

Launder, B. E., and Spalding, D. B. (1974). The Numerical Computation of Turbulent Flows. *Computer Methods in Applied Mechanics and Engineering.* **3**:269-289.

Lien, F. S., and Leschziner, M. A. (1994). Assessment of Turbulence-Transport Models Including Non-Linear RNG Eddy-Viscosity Formulation and Second-Moment Closure for Flow Over a Backward-Facing Step. *Computers in Fluids.* **23**:983-1004.

Papageorgakis, G. C., and Assanis, D. N. (1999). Comparison of Linear and Nonlinear RNG-Based k-ε Models for Incompressible Turbulent Flows. *Numerical Heat Transfer, Part B.* **35**:1-22.

Sheen, H. J., Chen, W. J., and Wu, J. S. (1997). Flow Patterns for an Annular Flow Over an Axisymmetric Sudden Expansion. *Journal of Fluid Mechanics.* **350**:177-188.

Shyy, W., Thakur, S. S., Ouyang, H., Liu, J., and Blosch, E. (1997). *Computational Techniques for Complex Transport Phenomena.* pp. 163-230. Cambridge University Press, Cambridge, UK.

Smith, L. M., and Reynolds, W. C. (1992). On the Yakhot-Orszag Renormalization Group Method for Deriving Turbulence Statistics and Models. *Physics of Fluids A*, **4**:364-390.

Taylor, B. N., and Kuyatt, C. E. (1994). Guidelines for Evaluating and Expressing the Uncertainty of NIST Measurement Results. NIST Technical Note 1297. National Institute of Standards and Technology, Gaithersburg, MD, 20899.

Widmann, J. F., Charagundla, S. R., Presser, C., and Heckert, A. (1999a). Benchmark Experimental Database for Multiphase Combustion Model Input and Validation: Baseline Case. NISTIR 6286. National Institute of Standards and Technology, Gaithersburg, MD 20899-8360, USA.

Widmann, J. F., Charagundla, S. R., and Presser, C. (1999b). Benchmark Experimental Database for Multiphase Combustion Model Input and Validation: Characterization of the Inlet Combustion Air. NISTIR 6370. National Institute of Standards and Technology, Gaithersburg, MD 20899-8360, USA.

Yakhot, V., and Orszag, S. A. (1986). Renormalization Group Analysis of Turbulence: I. Basic Theory. *J. Scientific Computing*, **1**:1-51.

Yakhot, V., Orszag, S. A., Thangam, S., Gatski, T. B., and Speziale, C. G. (1992). Development of Turbulence Models for Shear Flows by a Double Expansion Technique. Physics of Fluids A. **4**:1510-1520.

Yakhot, V., and Smith L. M. (1992). The Renormalization Group, the ε-Expansion and the Derivation of Turbulence Models. *Journal of Scientific Computing*. **7**:35-61.

Yin, M., Shi, F., and Xu, Z. (1996). Renormalization Group Based k-ε Turbulence Model for Flows in a Duct with Strong Curvature. *International Journal of Engineering Science*. **34**:243-248.